

Multiple thermohaline states due to variable diffusivity in a hierarchy of simple models.

Neil R. Edwards¹ and John G. Shepherd²

1. *L.E.G.I. Grenoble, France*

2. *Southampton Oceanography Centre, U.K.*

January 22, 2001

Abstract

The effect of variable vertical diffusivity is investigated in dynamically reduced models of the thermohaline circulation in a rectangular basin. In a simple box model, sufficiently strong variation of the diffusivity κ_v with stability G can lead to the existence of two stable equilibria. Related behaviour is found in well-resolved frictional geostrophic (FG) models. A hierarchy of under-resolved FG models is constructed, the simplest of which is an eight-cell cube, to connect the two extremes of resolution. Multiple solutions in low-order models are found to correspond to the formation of high-gradient layers which are unlikely to be resolved by current ocean models. Physical arguments show that layering and multiple solutions require κ_v to decrease more rapidly than $1/G$ and sensitivity experiments suggest that, in addition, κ_v must vary by a factor of 10 to 100.

In two-hemisphere runs with salinity forcing included, the dependence of diffusivity on stratification is found to marginally favour equatorially symmetric states. Finally, such variation is shown to have a profound effect on the periodic, flush-collapse cycle under strong saline forcing; specifically, if diffusivity is taken to be a function of stratification rather than depth, regime transitions can occur much more easily. It will therefore be important for climate modelling to determine which is more realistic.

keywords ; thermohaline circulation, diffusivity

1 Introduction

It has been known since the work of Bryan (1987) that the strength of the thermohaline circulation should depend fairly strongly on the magnitude of diapycnal mixing in the ocean but direct estimates of the mixing coefficient κ_d have been difficult to obtain, even as global or basin-scale averages. The possible effects of variable mixing rates have consequently received little attention. However, recent theoretical work (Munk and Wunsch 1998) has generated renewed interest in the physical basis of diapycnal mixing, and direct observations (Polzin *et al.* 1997, Watson *et al.* 1999) have shown for the first time that the rates can be highly variable even in the ocean interior. Variations in diapycnal mixing imply related variations in stratification, both locally and in basin average, as is clear from the simple one-dimensional balance of Munk (1966). Variations in stratification are, in turn, likely to result in variations in diapycnal mixing, since most physical

processes involved in mixing, including nonlinear internal wave interactions, internal wave breaking and double-diffusive processes, have some dependence on stratification. Thus the strengths of stratification and of diapycnal mixing both vary widely in the ocean but the relationship between the two is not well known except in restricted cases.

Polzin *et al.* (1997) found κ_d to be approximately constant over two decades of variation of density gradient G in internal wave fields where the energy spectrum conformed approximately to the empirical Garrett-Munk spectrum (Garrett and Munk 1975), typically within the main thermocline away from regions of double-diffusive or convective activity or strong currents. Diffusivities varying by a factor of 10 were found in a sequence of studies by Watson *et al.* (1999), Ledwell *et al.* (1993) and Ledwell *et al.* (1998) associated with a factor 40 variation in G , with low diffusivity associated with strong stratification. However, the principal findings of Polzin *et al.* (1997) were that mixing in the main thermocline can be very weak (around $10^{-5} \text{ m}^2 \text{ s}^{-1}$) and that variations in mixing appear to be strongly related to variations in bottom topography. Values were found to increase by 1 or 2 orders of magnitude above the mid-Atlantic ridge and enhanced mixing extended hundreds of metres above the ocean floor. This raises the possibility that tides may be an important source of energy for mixing, with dissipation spread over significant vertical regions by internal wave propagation.

Shifting the emphasis from the effects to the causes of mixing, the model of Munk and Wunsch (1998) postulates that mechanical work by tides creates a buoyancy flux which would lead to a diffusivity inversely proportional to density gradient if the rate of working were invariant. As a first estimate of the effects of such an assumption, Huang (1999) considered the effects on simple thermohaline circulation models of specifying a constant energy source for mixing as opposed to the usual constant diffusivity. It is however plausible that the rate of working might be reduced under strong stratification, resulting in an even more rapid decrease of diffusivity with stratification.

In summary, mixing rates are now known to be highly variable in the ocean. The mechanisms for this variation are, as yet, poorly understood. The largest variations so far found appear to be related to bottom topography but are likely to be affected by variations in stratification via changes in wave propagation parameters. Mixing rates due to other processes, such as double-diffusive instabilities and the averaged effects of convective events, strong currents and storms are less well known. An overall average relation between stratification G and diffusivity κ_d therefore remains a subject of conjecture.

Our aim in this paper is to consider the possible effects of strong variation of κ_d . An important issue is the extent to which variations in κ_d can be parameterized in terms of variations in G in simple models. Specifying purely spatial variation could prevent models from reacting properly to changes in external forcing and inhibit switches between flow regimes, whereas specifying overly strong variation of κ_d with stratification could overestimate the effect of internal feedbacks and instabilities within the flow.

We have therefore been motivated to undertake some exploration of the effects of variable mixing on the thermohaline circulation (THC), and on the possible generation of multiple stable states in some simplified models. In particular, it seems possible in principle that

(a) a reduction of κ_d in highly stratified regions might suppress local diapycnal motion, and thus contribute to the known instability of equatorially symmetric upwelling (thermally driven) modes in ocean models,

(b) sufficiently strong variation of κ_d might generate a new class of possible alternative stable states of the THC, not dependent on the familiar mechanism of opposing thermal and haline forcing, first discussed by Stommel (1961).

We note in passing that whilst for many purposes the global (or basin-wide) average of κ_d captures the essence of variations of the THC, the local balance of advective and diffusive processes (including convection) requires that the spatial structure of any steady-state density field, and thus of the THC, will depend on the spatial variation of κ_d whether determined by local physical forcing (e.g. tidal friction) or variations of stratification.

The possible effects of strong dependence of κ_d on stratification are therefore explored below, firstly in the context of a simple box model, and then in the context of less over-simplified three-dimensional “thermocline” models with frictional geostrophic (FG) dynamics. Initial experiments with well-resolved FG models showed somewhat different behaviour from the box model, motivating the construction of a hierarchy of FG models to bridge the gap in complexity as smoothly as possible. This exploration of the effects of stability-dependent diffusivity in a hierarchy of models involves highly idealised representations, and is intended to complement investigations using more realistic models such as that of Manabe and Stouffer (1999).

The outline of the paper is therefore as follows; we first discuss the behaviour of the box model, then the basic FG model and its reduction to a hierarchy of models of varying resolution. In the following section, 6, we trace the effect of variable diffusivity in FG models of increasing resolution. Section 7 then considers the effect of variable diffusivity on the stability of pole-to-pole circulation modes in a two-hemisphere configuration with both thermal and saline forcings. Section 8 considers the time-dependent solutions which result when the saline forcing is strong. The results are discussed in Sections 9 and 10. The extent to which our findings have relevance to the real world will depend on the true strength of any dependence of κ_d on stratification, on which we may expect new theoretical and experimental results in the foreseeable future.

2 A plausibility argument in a minimal box model

To investigate the effect of variable vertical diffusivity on the thermohaline circulation we start by considering the minimal box model depicted in Figure 1. The model represents a single-hemisphere ocean basin by means of one homogeneous polar box of temperature T_p and two homogeneous mid-latitude boxes, an upper “equatorial” box of temperature T_e and a deep water box of temperature T_d . For simplicity we assume that the mid-latitude boxes have depth $H/2$ and length $L/2$ while the polar box has depth H and length $L/2$. We assume that surface forcing maintains the temperatures T_e and T_p at fixed values, and that there is a density-driven circulation in the sense indicated, with flow rate q into the deep water box. Following the usual procedure of upstream differencing for advection, and allowing for a vertical diffusivity κ between the equatorial and deep water boxes, we can write the equation for T_d as

$$\frac{d}{dt}T_d = \frac{q}{L}(T_p - T_d) + \frac{2\kappa}{H^2}(T_e - T_d). \quad (1)$$

The flow rate q has to be parameterized in terms of the north-south temperature, and hence pressure, difference. For the moment we simply take $q = \beta(T_d - T_p)$, where β is a constant, although in general we might expect the flow rate to depend on the depth-integrated north-south density difference, here this would merely introduce the constant factor $(T_e - T_p)$. We refer to this modification below. We still have to define a form for κ which will be taken to be some decreasing function of the temperature difference $(T_e - T_d)$, to represent in a very general way the inhibition of vertical mixing by increased

stratification. From equation (1) the condition for a steady state is

$$\frac{\beta}{L}(T_p - T_d)^2 = \frac{2\kappa}{H^2}(T_e - T_d). \quad (2)$$

Non-dimensionalising the temperature differences by the surface temperature difference $(T_e - T_p)$, we can reexpress this condition succinctly as an equation for the dimensionless stratification parameter $d = (T_e - T_d)/(T_e - T_p)$. The resulting equation is

$$(1 - d)^2 = kf(d)d, \quad (3)$$

where k is a dimensionless measure of the relative strength of advection and diffusion and the dimensionless function $f(d)$ gives the dependence of the diffusivity on d . The correct form for $f(d)$ is not well known (see Section 9). Our aim here is simply to investigate the possible effects of allowing the diffusivity to decrease with increasing stratification. Therefore to proceed, we choose at this point the function

$$f(d) = 1/(1 + \epsilon d/n)^n, \quad (4)$$

for some choice of the parameters ϵ and n . Figure 2 gives a graphical solution of equation (3) for $n = 3$, $\epsilon = 24$ and $k = 30, 50$ and 80 . It is clear from the graph that, depending on the choice of parameters, equation (3) may have up to 3 solutions, corresponding to 3 stationary points of the system. Further, if the equation does have 3 solutions, then 2 of these will be stable and one unstable. Thus in our simple box model, the introduction of variable vertical diffusivity can lead to the existence of multiple stable steady states, even in a single hemisphere model with only a single active tracer. The simplicity of our model serves to clarify the mechanism for the possible existence of the two stable states; the solution with smaller stratification d has larger advective and diffusive heat flux into the deep water box, faster flow and warmer deep water. The solution with larger stratification has relatively smaller fluxes as a result of the increased stratification, slower flow and cooler deep water.

Even in the context of box models, this model involves some extreme assumptions. Amongst the most questionable of these is the proportionality between flow rate and deep temperature gradient. However, if we allow for a more general dependence on the integrated north-south temperature gradient $q = \beta(T_d - T_p) + \beta'(T_e - T_p)$, the left hand side of equation (3) can still be written as $(1 - d)(1 - \alpha d)$, for some constant α , and the possibility of multiple solutions, for appropriate choice of parameters, remains. Another rather bold assumption, that the temperatures T_e and T_p remain fixed, corresponds to the limit of strong relaxation towards apparent atmospheric temperatures. Given standard box model formulae, such as those given by Thual and McWilliams (1992), it can easily be shown that this assumption can be relaxed without necessarily affecting the possible existence of multiple solutions.

The details of the box model are somewhat tangential to our argument, since our aim in this section is to illustrate a possible mechanism in order to motivate a search for related behaviour in a more complex model, specifically a frictional geostrophic model. Whether the phenomenon of multiple states seen in the box model is relevant to the real ocean will depend critically on whether the form of the diffusivity is realistic. As already noted, we will not attempt to address this issue directly in this paper, even for the more complex models. To some extent we present an inverse perspective, by investigating how the vertical diffusivity would need to vary in order to produce the behaviour which we describe.

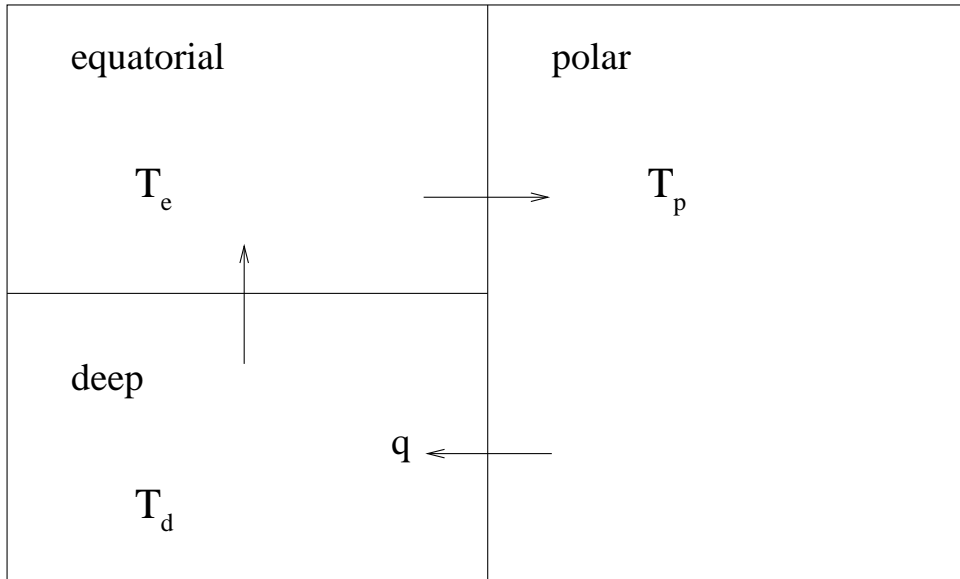


Figure 1: Diagram of the box model.

3 The frictional geostrophic model

Our numerical model is based on the thermocline (or planetary geostrophic) equations with the addition of a linear drag term in the horizontal momentum equations. We therefore refer to the model as a frictional geostrophic (FG) model. The density depends nonlinearly on the local values of temperature T and salinity S , which obey separate advection-diffusion equations and are also subject to convective adjustment. Apart from changes to the boundary conditions and the time-stepping procedure, described in the Appendix, the model is essentially as used by Edwards, Willmott and Killworth (1998), and is described more fully therein.

Referred to spherical polar coordinates (ϕ, s, z) , where ϕ is longitude, $s = \sin \theta$, θ is latitude and z is measured vertically upwards, the governing equations can be expressed in the dimensionless form

$$-sv = -\frac{1}{c} \frac{\partial p}{\partial \phi} - \lambda u, \quad (5)$$

$$su = -c \frac{\partial p}{\partial s} - \lambda v, \quad (6)$$

$$\frac{\partial p}{\partial z} = -\rho, \quad (7)$$

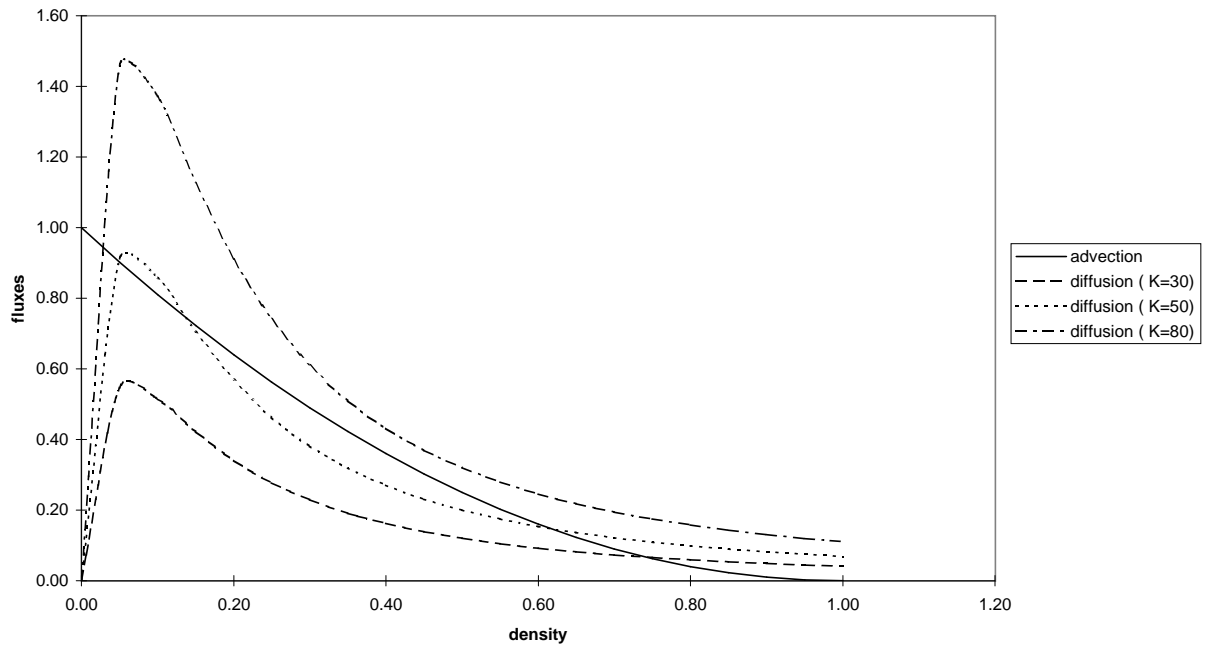
$$\frac{\partial}{\partial \phi} \left(\frac{u}{c} \right) + \frac{\partial}{\partial s} (vc) + \frac{\partial w}{\partial z} = 0, \quad (8)$$

$$\rho = \rho(S, T), \quad (9)$$

$$\frac{D}{Dt} X = \kappa_h \nabla^2 X + \frac{\partial}{\partial z} \left(\kappa_v \frac{\partial X}{\partial z} \right) - \mu \nabla^4 X + \mathcal{C}. \quad (10)$$

In the above, $c = \cos \theta$ and λ is the drag coefficient. Horizontal lengths have been scaled by the Earth's radius r_0 ; vertical lengths by a typical mid-ocean depth H ; the horizontal velocity components (u, v) in the (ϕ, s) directions have been scaled by a typical horizontal velocity U ; and the vertical velocity w has been scaled by UH/r_0 . The scalings for the

Figure 2: Graph illustrating the possibility of multiple solutions to equation (3), representing multiple steady states in the box model. The ordinate is proportional to the heat flux into the deep water box.



perturbation pressure p and density ρ are derived from the geostrophic and hydrostatic relations respectively. The density gradient $G = \partial\rho/\partial z$ is therefore scaled by $\rho_0 f U r_0 / g H^2$ where ρ_0 is a reference density and f is twice the Earth's angular velocity. Quantity X in equation (10) represents either temperature T or salinity S and D/Dt is the material derivative. Scalings for S and T are not necessary because they appear linearly in equation (10); their magnitudes depend on the boundary forcing. The advective time scale r_0/U is used. \mathcal{C} is the convective adjustment term, which acts to remove static instability while conserving S and T . The state equation for the dimensional density ρ_* takes the form

$$\rho_* = 1000 + 0.7968S - 0.0559T - 0.0063T^2 + 3.7315 \times 10^{-5}T^3, \quad (11)$$

which closely approximates the UNESCO formula for observed ocean density in kg m^{-3} if S is in practical salinity units (psu) and T in degrees Celsius (Gill 1982). In this and several other respects we follow Winton and Sarachik (1993), who used a similar model to study long-period oscillations of the thermohaline circulation.

These equations can satisfy a boundary condition of no normal flow at all boundaries. With the introduction of the biharmonic operator ∇^4 in equation (10), it is mathematically consistent to impose a condition of zero heat and salt fluxes through the lateral boundaries, although in practice we will set the coefficient μ to zero in the runs described below (see Appendix). The lower boundary fluxes of T and S are also set to zero while at the upper boundary mixed Dirichlet / Neumann type boundary conditions are used to give the required thermohaline forcing. Wind forcing can be included as a source term in equations (5) and (6) but will be ignored for simplicity in this study.

The flux of temperature out of the top grid box is given by

$$F_T = -\frac{T_a - T}{\tau_r} \Delta z, \quad (12)$$

where Δz is the depth of the top grid level, T is the temperature in the top grid level, τ_r is a restoring timescale, and the prescribed apparent atmospheric temperature T_a is a cosine function of latitude given by

$$T_a = A \cos\left(\frac{\pi\theta}{2\theta_1}\right), \quad (13)$$

where the domain has been assumed to extend from latitude θ_0 to θ_1 with a longitudinal extent of L_ϕ and the constant $A = 25$, so that model temperature values can be taken to be in degrees Celsius. The surface salinity flux is defined as the gradient of a northward salinity transport, and is given by

$$F_S = \frac{D}{L_\phi} \frac{\partial}{\partial s} \left(\sin\left(\frac{\pi\theta}{\theta_1}\right) \right) \quad (14)$$

where the constant D is chosen so that the model salinity unit can be taken to be equivalent to 1 psu. Diffusion parameter values have generally been kept as small as possible consistent with numerical stability.

The equations are discretized on an Arakawa 'C' grid using simple, second order, centred differences in space. The resulting form for the tangential velocity value closest to the boundary, which is one half grid cell from the boundary itself, requires the density to be defined at adjacent land points to calculate the normal derivative of pressure. At high resolution the required density values can be found by integrating the condition of

Table 1: Default parameter values.

parameter	value	dimensional equivalent
A	25	25 ⁰ C
θ_0	10 ⁰	–
θ_1	70 ⁰	–
L_ϕ	60 ⁰	–
D	7.85×10^{-3}	10 ⁷ psu m ³ s ⁻¹
λ	6.35×10^{-2}	(1.25 days) ⁻¹
κ_h	9.42×10^{-3}	3000 m ² s ⁻¹
κ_v	7.96×10^{-4}	10 ⁻⁴ m ² s ⁻¹
τ_r	4.14×10^{-2}	61 days

zero normal velocity around the boundary as described in the Appendix, but at very low resolution we use a simpler method (see below). A simple forward difference in time provides adequate accuracy, since the time step is limited by numerical constraints, and is twice as efficient as a centred difference in time, since the allowed time step is longer. At each time step the velocity field is determined diagnostically from the density field, and then relaxed back to the velocity used at the previous timestep as described in the Appendix. In the absence of wind and topographic forcing the depth integral of the velocity can be assumed to be zero.

The equations are solved in a 60⁰ wide sector of constant depth H . For the single-hemisphere runs the domain extends from 10⁰ to 70⁰ North, while for the cross-equator simulations the northern and southern boundaries are set at $\pm 60^0$. Model vertical levels are uniformly spaced in the logarithmic coordinate $\zeta = \log(1 - z + 0.1)$ so that the upper layers are thinner, while the horizontal grid is uniform in the (ϕ, s) , longitude sin(latitude) coordinates (giving boxes of equal area in physical space).

The default values of all the above parameters and their dimensional equivalents, where appropriate, are given in Table 1. Dimensional values have been obtained using a velocity scale $U = 0.05$ m s⁻¹ and a depth scale $H = 4000$ m, which gives a time scale of 4.04 years and a scale for the overturning streamfunction of 1274 Sv. The scale for the density gradient G is 2.96×10^{-4} kg m⁻⁴. The default constant value of κ_v is later referred to as κ_{v0} (note that in the n -cube runs described below the diffusivities κ_h and κ_v are multiplied by a factor $(16/n)^2$).

4 Reduction of the FG model to a hierarchy of low-order models

Although the dynamics of the FG model are considerably simpler than those of standard primitive equation ocean models, there is still a considerable gap in complexity between the FG model and the box model of section 2. Formally, the FG model is derived on the assumption that the numerics are adequate to resolve the continuous equations, thus a well-resolved simulation will have many degrees of freedom, whereas our box model has only 1. To attempt to bridge this gap in complexity as smoothly as possible, and hopefully facilitate the transfer of dynamical insight from one system to the other, we perform a

rather radical reduction of the FG model resolution to generate a hierarchy of low-order models. Here we describe the modifications which are necessary to allow us to apply the resulting hierarchy of models to the current problem of variable vertical diffusivity in the thermocline. For other problems it may be necessary to make further modifications to tune the dynamics and behaviour of the lowest order models. In such a case it may be of interest to perform a more detailed analysis of the behaviour of the hierarchy and of the effect of radically changing the resolution, but we do not attempt to do so here. Indeed, it seems likely that such difficult choices as where to put the necessary changes in parameterizations and which parameters to vary would, in fact, very much depend on the details of the application,

The lowest order model obtainable by changing the resolution of the FG model, without re-parameterizing the essentially three-dimensional dynamics, is an 8-cell cube in the computational domain with two grid cells in each direction. We refer to this configuration as a 2-cube. Similarly we will refer to an n -cube for n a positive integer. In practice we will restrict attention to such n -cubes to keep our discussion within reasonable bounds, since our intention is merely to illustrate the behaviour of the hierarchy, rather than to attempt an exhaustive investigation of the vast range of possible choices of resolution.

Adjacent to boundaries in the FG model the tangential velocity depends on the normal derivative of pressure. At high resolution the required derivatives are calculated by integrating the condition of zero normal velocity around the boundary (see Appendix). At very low resolution it becomes questionable to strongly constrain the tangential velocities in this way, by using a relation which is only strictly valid at the boundary, since the tangential velocities involved may be further from the boundary than the width of any realistic boundary layer. For very low resolution (in practice for $n \leq 4$) we therefore calculate the required normal derivatives using a simple first order difference, which amounts to retaining our standard discretization of the normal derivatives with the required, across-boundary density values determined using linear extrapolation in place of the boundary integral equation. This was found to give a much smoother velocity field for $n \leq 4$, while for $n \geq 8$ the integral method allows a much shorter time step (see Appendix).

Changes to the resolution of the model should be accompanied by changes to the dissipative parameter values, to maintain numerical stability but also to represent the change in the range of resolvable dissipative physical processes. Since the former consideration is dominant at very coarse resolution we keep the diffusion values as low as is reasonable for the resolution. On dimensional grounds, for the runs described below, the horizontal and vertical diffusivities are made to increase in proportion to the square of the longitudinal grid spacing. Values are normalised to those given in Table 1 for n equal to 16. Thus for $n < 16$ the values given in the Table are multiplied by a factor $(16/n)^2$. It is important to increase the dissipation sufficiently to maintain the cell Peclet numbers at reasonable values. (The cell Peclet number is defined by $Pe = w\Delta z/\kappa_v$ for the vertical direction, where Δz is the vertical grid size, and similarly in the other directions.) For Peclet number $Pe > 2$ second order central differences for advection and diffusion can result in a form of overshoot, leading to temperatures which are outside the range of neighbouring values. Discontinuously changing the discretization of advection to an upwind scheme at low resolution would cure this problem since 1st order upwind differencing is equivalent to 2nd order differencing with the addition of a large but variable diffusivity which is such as to maintain $Pe = 2$. However this would reduce the continuity of the model hierarchy and remove any effective spatial control over diffusion values, which is undesirable in a study of the effect of spatially variable diffusivity. For simplicity, however, we keep the

frictional parameter λ at a constant value consistent with a boundary layer of order one grid point wide at $n = 16$.

5 The standard solution for the 2-cube

For the parameters given above, the steady solution of the 2-cube with constant κ_v is shown schematically in Figure 3. Values in circles are the temperatures in the appropriate grid cells, arrows between circles indicate the direction of the velocity components, labelled with their respective magnitudes. Note that the vertical grid is stretched while the horizontal grid is uniform in the (ϕ, s) , longitude $\sin(\text{latitude})$ coordinates. The vertically integrated horizontal mass flux at every point is zero. The solution shows some familiar characteristics; the north-south temperature gradient in the upper layer resulting from the surface forcing drives a zonal overturning flow, by geostrophy, which is eastward at upper levels and westward below. The resulting vertical advection cools the western side of the domain giving rise to a secondary circulation which is the expected meridional overturning circulation with downwelling in the north. Advection and diffusion in the sinking region cannot maintain static stability there and both northern columns are convecting. Less realistic is the lack of westward velocity intensification, and the consequent anticlockwise horizontal recirculatory component to the upper layer flow. In practice the difference between the eastward velocity components in the upper level is mostly a result of the geometry, since both “feel” the same zonally averaged meridional density gradient in the Coriolis term, and the drag force, which is westward at this level, is a much smaller term. It is interesting to note that the diffusivities are not quite sufficient to prevent a fractional overshoot in the south-west, lower-layer temperature, which is the lowest in the domain. This is the result of a vertical Peclet number slightly greater than 2 (average 2.6) which suggests, as noted above, that the implied numerical diffusivity which would be generated by an upwind vertical advection scheme in this case would be even greater than that used here, which equates to a dimensional value of $64 \times 10^{-4} \text{ m}^2 \text{ s}^{-1}$, given our assumed dependence on grid spacing. The diffusion time scale H^2/κ_v controls the time taken to reach equilibrium. Thus the 2-cube converges rapidly and by time $t = 100$ the numerical solution has ceased to change.

6 The effect of variable diffusivity

The aim of this section is to search for multiple solutions induced by variable vertical diffusivity in the hierarchy of FG models, analogous to those in the box model of section 2. In doing so we will illustrate some aspects of the behaviour of the FG hierarchy. As observed in the introduction, initial experiments with the FG model suggested that multiple steady states were not a ubiquitous feature of variable vertical diffusivity experiments and that it was necessary to consider carefully the correspondence between the box model and the FG model to understand the phenomenon. We therefore turn first to the 2-cube, which we would expect to exhibit very similar behaviour to the box model. Throughout this section we will ignore the effect of salinity and consider solutions forced only by surface heating and cooling.

6.1 Multiple solutions in the 2-cube

In the 2-cube the vertical diffusivity κ_v is required at only one vertical level at each of the 4 horizontal interfaces between upper and lower cells. Allowing κ_v to depend on the local vertical density gradient G does not, therefore, permit κ_v to vary in the vertical, but only with time and horizontal position. Regarding horizontal variation we have seen, in a particular steady solution (but the result holds for a range of diffusivities), that upwelling only occurs at two of the 4 horizontal interfaces, one of which is in a convecting column. Thus there is only one interface across which vertical advection and diffusion of heat can be in approximate balance; the classical thermocline balance assumed in the box model of section 2. It seems likely that the details of the solution will depend strongly on the value of κ_v at this upwelling interface and less strongly on its value at the other interfaces. In other words, a steady solution of the 2-cube with variable $\kappa_v(G)$, in which the value of $\kappa_v(G)$ at the upwelling interface is κ_{vu} , may differ only slightly from a steady solution with κ_v constant and everywhere equal to κ_{vu} . If so it should be possible to produce multiple steady states in the 2-cube by the following procedure: first find the value G_u of the density gradient at the upwelling interface in the steady solution for fixed diffusivity κ_v ; then repeat this process for a range of values of κ_v to derive a functional relationship $G_u(\kappa_v)$ characterising the behaviour of the model at constant κ_v ; then define a function $\kappa_v(G)$ which agrees with $G_u(\kappa_v)$ at several points, that is the graphs of the two functions intersect at several points; finally look for solutions to the 2-cube using the new function $\kappa_v(G)$ (at all 4 points) with a suitable range of initial conditions. Steady solutions to the 2-cube with variable κ_v should occur close to any points which lie on the derived graph $G_u(\kappa_v)$, that is close to the intersection points of the two graphs. We would expect at least two of the intersections to correspond to stable steady states if there are three or more such intersections. We illustrate this procedure by example below.

Firstly we run the 2-cube FG model to a steady state with constant κ_v for a range of values of κ_v from 0.051 (corresponding to the standard value κ_{v0} given in Table 1 scaled by the grid spacing) to $\kappa_v = 5.1$. In each case we diagnose the value of the density gradient G in the south west grid column, which is the upwelling column most reminiscent of the classical thermocline. The resulting function $G(\kappa_v)$ is plotted in Figure 5.

Significantly, the density gradient G varies by a factor less than 10 while κ_v varies by a factor of 100. The implication of this is that the inverse function $\kappa_v(G)$, which we now wish to define, must vary strongly with G in order to cut the graph $G(\kappa_v)$ in at least 3 places. An example function which does so is the step-like tanh function given by

$$\kappa_v = \kappa_{\min} \left(1 + \frac{1}{2} (r - 1) (1 - \tanh(a(G - G_0))) \right) \quad (15)$$

which is plotted in Figure 5 for $\kappa_{\min} = 0.051$, $r = 100$, $a = 10$ and $G_0 = 1.5$. This function crosses the diagnosed curve $G_u(\kappa_v)$ at the maximum and minimum values of κ_v plotted and also at $G \approx 1.5$. Our hypothesis is that the 2-cube with variable vertical diffusivity given by this function will have 2 stable steady states close to the two extreme intersection points of the two graphs; one with $\kappa_v \approx 0.051$ and $G \approx 3.7$ at the south west interface and one with $\kappa_v \approx 5.1$ and $G \approx 0.44$ there. A third stationary point corresponding to $G \approx 1.5$ is expected to be unstable and thus not obtainable numerically.

A given integration of the time-dependent FG model will converge if the instantaneous state of the model comes sufficiently close to a stable steady state. The choice of initial conditions will determine which steady state is obtained if more than one exists. If different steady states are characterised by different basin-averaged temperatures we might anticipate being able to reach different states starting from a condition of uniform

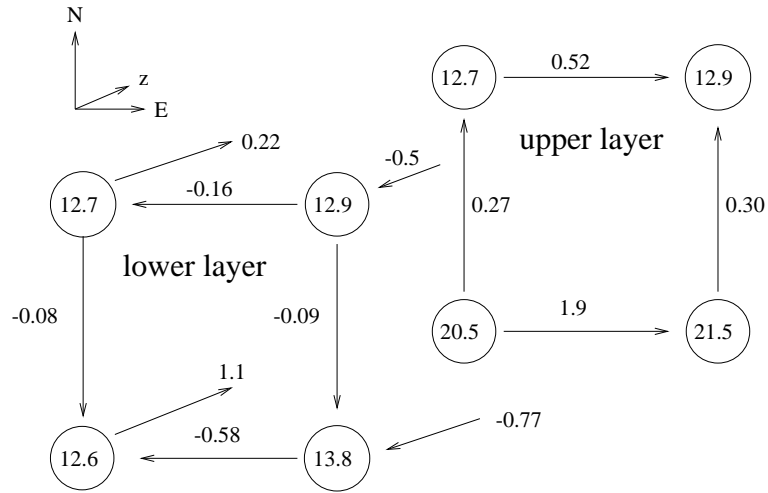


Figure 3: Steady state in the 2-cube. Values in circles are the temperatures at each grid cell, arrows indicate direction of velocity components between cells, labelled with appropriate magnitudes. Orientation is as shown in the upper left of the figure.

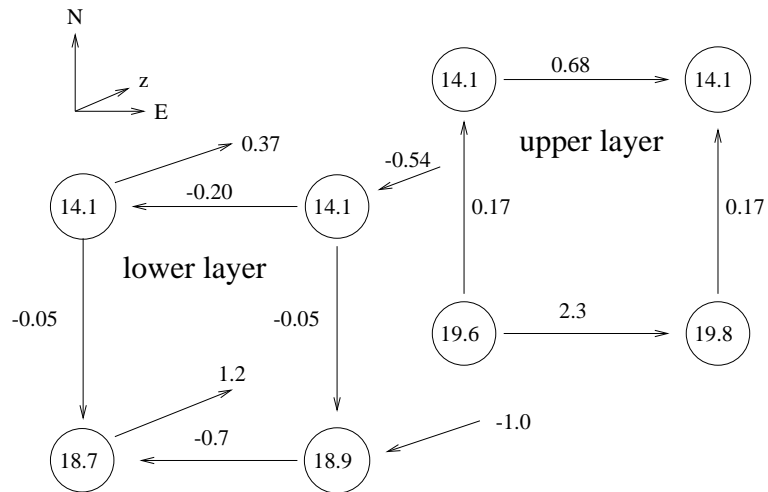


Figure 4: Alternative steady state in the 2-cube for variable diffusivity and warm initial condition. Values in circles are the temperatures at each grid cell, arrows indicate direction of velocity components between cells, labelled with appropriate magnitudes. Orientation is as shown in the upper left of the figure.

temperature T_0 by varying the value of T_0 . If T_0 is large, that is close to the maximum value of apparent atmospheric temperature T_a , the initial response of the model is strong northern convection leading to strong meridional flow. If T_0 is close to the minimum value of T_a the thermocline develops slowly by diffusion and the meridional flow builds up accordingly. Thus a large value of T_0 should favour the solution with stronger flow and warmer deep water, while a small value of T_0 should favour the solution with weaker flow and cooler deep water. Using the function $\kappa_v(G)$ given above and plotted in Figure 5 we have integrated the 2-cube starting from $T_0 = 0$ and starting from $T_0 = 25$ and indeed we find two distinct steady states with different deep temperatures and different amounts of overturning. Closer examination confirms that the two solutions are indeed close to the two constant κ_v solutions corresponding to the two extreme intersection points of the two graphs in Figure 5, as hypothesised above. In fact they are essentially indistinguishable. With a cold start we obtain the solution already plotted in Figure 3. The hot-start run is shown in Figure 4. The exact correspondence between the constant and variable κ_v solutions is largely due to the sharpness of the step function $\kappa_v(G)$. In the hot-start run, G is small at all 4 points and κ_v takes its maximum value. With a cold start G is large in the southern, thermocline-like region ($G \approx 4$) and κ_v takes its minimum value. The large value of κ_v at the two northern points in this solution has no dynamical effect, since the vertical density gradient is zero there. Thus the solution is identical to one with small κ_v everywhere. The result of using different forms for $\kappa_v(G)$ will be discussed in Section 9.

The 2-cube FG model can thus be made to behave similarly to the 3-box model of section 2. For a sufficiently sharply decreasing function $\kappa_v(G)$ the model exhibits multiple stable steady states. One steady state has weak stratification and warm deep water, and another solution exists with strong stratification and cool deep water. According to the 3-box model the weakly stratified solution should have a stronger meridional overturning, but on this point the models disagree. The 2-cube has just sufficient complexity to allow the meridional overturning flow to develop by geostrophy (as described in section 5) through the action of the zonal overturning on the vertical density gradient. The weakly stratified solution does have a stronger zonal overturning (compare Figures 3 and 4) but because the stratification is weaker this does not lead to a stronger meridional overturning. In fact the value of the meridional overturning is 0.034 (43 Sv) in the hot-start, weakly stratified case, and 0.057 (73 Sv) in the cold-start, strongly stratified case.

6.2 Multiple solutions with more degrees of freedom

(i) *The 3-cube.* Progressing through our hierarchy of n -cube FG models in search of multiple stable states we pass next to the 3-cube. This is possibly the least physically justifiable model of the thermohaline circulation. While the 2-cube has just sufficient freedom to represent the interaction between vertical stratification and recirculations parallel to the three coordinate planes, the extra degrees of freedom in the 3-cube lack a clear physical interpretation. This may be why Huang and Stommel (1992) had difficulty developing a low resolution box model including Coriolis forces. With the addition of wind forcing the ability of the 3-cube to represent 2 horizontal gyres could be significant, but for our purposes the significance of the 3-cube is that the diffusivity κ_v can vary in the vertical. Since the 3-cube has 27 nodal temperature values, it becomes easier to visualise the solutions using contour plots, always bearing in mind that each underlying 2-dimensional field has only 9 points. Figure 6 is just such a plot, indicating succinctly the variation of temperature and velocity at each horizontal level in the steady 3-cube solution with constant κ_v and the standard parameters (scaled as described) given in Table 1.

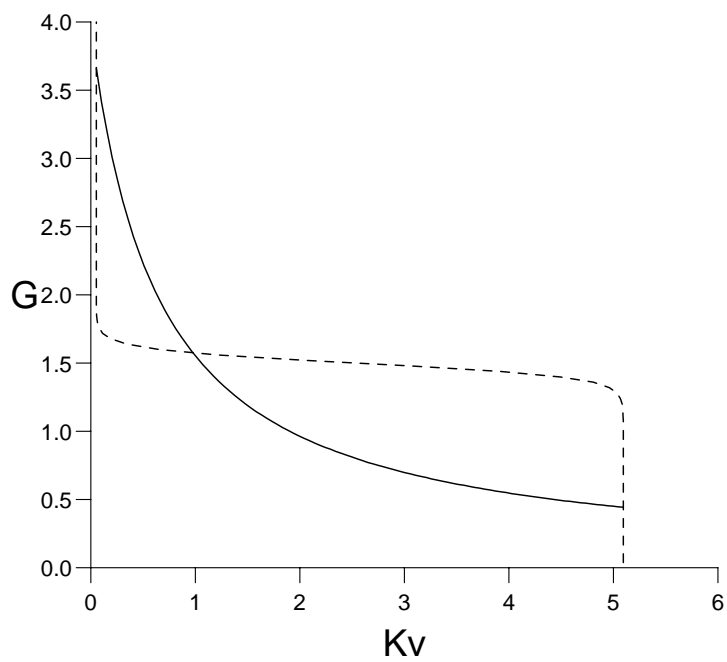


Figure 5: Density gradient G at the upwelling (south-west) interface against vertical diffusivity κ_v for steady solutions to the 2-cube with constant κ_v ; solid line. The analytical function $\kappa_v = 0.051(1 + 49.5(1 - \tanh(10(G - 1.5))))$ is shown dotted.

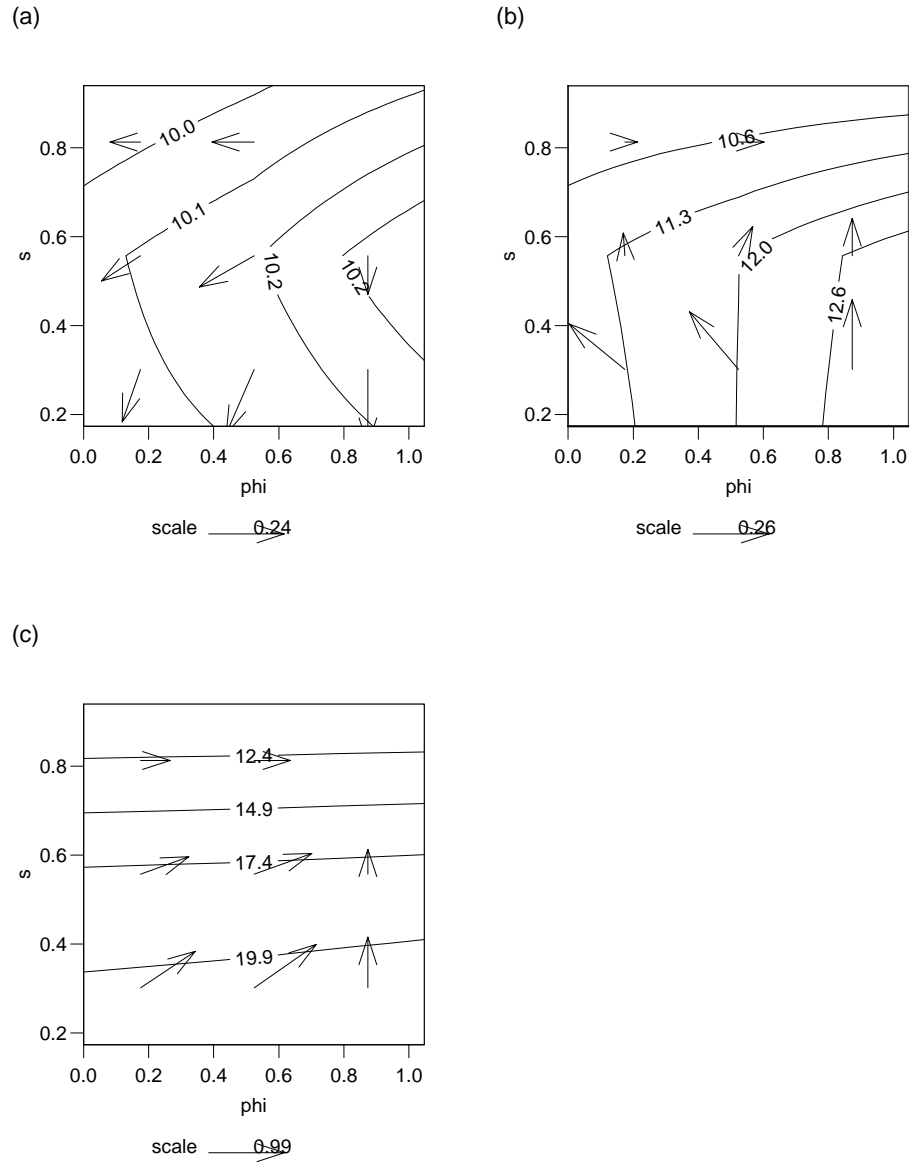


Figure 6: Contours of temperature and velocity arrows for a steady solution of the 3-cube with standard parameter values at each of the three model levels from the deepest (a) to the surface (c). Note that each field contoured has only 9 points, and that the velocity arrows represent the combination of 2 horizontal components which are not collocated on the model C-grid. ϕ is longitude and s is $\sin(\text{latitude})$.

In spite of the above reservations, the solution is remarkably well behaved, with sinking in the north and east and relatively uniform deep water, slightly cooler than in the standard solution to the 2-cube, with a minimum temperature of just below 10 in the vertically uniform northern convecting region.

Our inverse procedure for locating multiple solutions for the 2-cube does not extend easily to the 3-cube, in which G is defined at 18 different points. However, using again the function $\kappa_v(G)$ defined in equation (15) (with κ_{\min} again set to the standard value κ_{v0} given in Table 1 scaled by the grid spacing) we find that the possibility of vertical variation of κ_v does not prevent the model from exhibiting multiple steady solutions. Setting the initial constant temperature T_0 to 0, 15 and 25 produces 3 different solutions. All are qualitatively similar to the steady solution of Figure 6 but increasing the initial temperature results in progressively warmer deep water and reduced stratification. The change in meridional overturning between the three cases is not monotonic, the maximum value of the meridional overturning streamfunction Ψ_M in the steady state being 0.07 when $T_0 = 0$, decreasing to 0.05 for $T_0 = 15$, and increasing to 0.1 for $T_0 = 25$.

The difference between these three solutions is best expressed in terms of the diffusivity at the upper of the two interfaces. In these solutions the ratio γ of the vertical diffusivity κ_v to its minimum value κ_{\min} is everywhere almost exactly equal to 1 or r (here the ratio $r = 100$). At the lower interface the diffusivity ratio γ is equal to r everywhere but the values γ_{ij} at the (i, j) th point in the upper layer can be represented schematically in the three solutions as follows, where i is the ϕ index increasing eastwards and to the right and j is the s index increasing northwards and upwards.

$$\begin{pmatrix} r & r & r \\ 1 & 1 & 1 \\ 1 & 1 & 1 \end{pmatrix} : T_0 = 0, \quad \begin{pmatrix} r & r & r \\ r & r & r \\ 1 & 1 & 1 \end{pmatrix} : T_0 = 15, \quad \begin{pmatrix} r & r & r \\ r & r & r \\ r & r & r \end{pmatrix} : T_0 = 25. \quad (16)$$

Thus, as in the 2-cube, the different solutions correspond to the possibility of a strongly stratified layer at the surface in the south, but here the meridional extent of the stratified layer is variable, leading to an increased number of solutions. With hindsight we can understand the behaviour a little better by attempting the procedure applied above to the 2-cube and deriving the function $G(\kappa_v)$ for steady solutions with constant κ_v . Motivated by the structure of κ_v seen above, we average G zonally and ignore the values in the northernmost grid cells. The resulting 4 averaged values of $G(s, z)$ are plotted in figure 7 along with the function $\kappa_v(G)$. The Figure shows that G is always small in the lower layer in constant κ_v solutions, which is consistent with the large value of κ_v found in the lower layer in all of the variable κ_v solutions. The fact that G in the lower layer shows little variation across the range of constant κ_v is suggestive of an insensitivity of G to κ_v in the deep, which in turn suggests that solutions in which κ_v increases with depth may exist which are not dissimilar to solutions in which κ_v remains small throughout the water column.

(ii) *The 4-cube.* In an exactly analogous way we find 4 steady solutions for the 4-cube which can be summarised similarly in terms of their relative diffusivity γ_{ij} at the uppermost interface as follows.

$$\begin{pmatrix} r & r & r & r \\ 1 & 1 & 1 & 1 \\ 1 & 1 & 1 & 1 \\ 1 & 1 & 1 & 1 \end{pmatrix} : T_0 = 0, \quad \begin{pmatrix} r & r & r & r \\ r & r & r & r \\ 1 & 1 & 1 & 1 \\ 1 & 1 & 1 & 1 \end{pmatrix} : T_0 = 10, \quad (17)$$

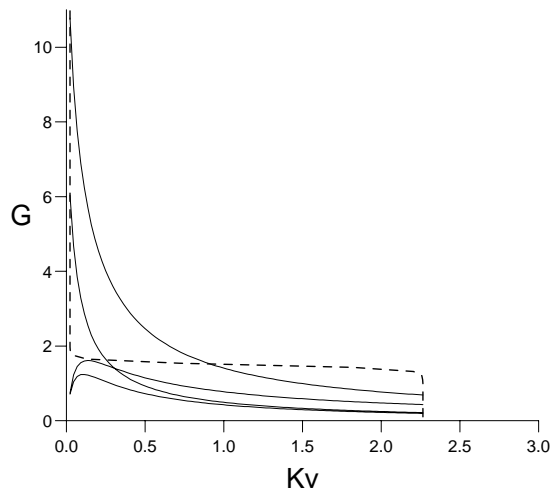


Figure 7: Zonally averaged values of density gradient G in steady solutions of the 3-cube with constant κ_v , solid lines; along with the function $\kappa_v(G)$, dashed. The upper 2 solid lines correspond to the upper interface and the lower lines the lower interface. Within each pair the lower line corresponds to the southern point and the upper the central point. Values for the northern points are not plotted.

$$\begin{pmatrix} r & r & r & r \\ r & r & r & r \\ r & r & r & r \\ 1 & 1 & 1 & 1 \end{pmatrix} : T_0 = 15, \quad \begin{pmatrix} r & r & r & r \\ r & r & r & r \\ r & r & r & r \\ r & r & r & r \end{pmatrix} : T_0 = 25. \quad (18)$$

Thus for $n=2,3,4$ each solution corresponds to a zonally uniform distribution of diffusivity with a single high-gradient layer at the surface of meridional extent between 1 and n points.

(iii) *The 8-cube.* For $n = 8$ the steady n -cube solution with constant κ_v , plotted in Figure 8, is fairly smooth, with some western intensification of currents visible. Recall that for $n > 4$ we use the more complex boundary condition discussed in the Appendix. Using the function $\kappa_v(G)$ given in equation (15) with κ_{\min} rescaled as before we can again find more than one steady solution. This time, however, an initial search reveals only 3 very similar solutions, all with high relative diffusivity $\gamma = r$ everywhere except the southern half of the top layer. This rather weaker form of multiplicity raises the possibility that better-resolved FG model solutions may not exhibit multiple solutions at all, but this turns out not to be the case.

(iv) *The 16-cube.* Doubling the resolution once again we conclude our discussion of the n -cube hierarchy with the 16-cube. The solution for constant κ_v is plotted in Figure 9. Any remaining non-smoothness of model velocity and temperature fields is probably as much an artefact of the reduced model physics as of the low resolution. Certainly the solution qualitatively resembles that for $n = 8$ even though the diffusion values used for $n = 8$ are four times as large. If we re-compute the 8-cube solution with the same constant diffusion values as the 16-cube, the maximum meridional overturning differs by only 5% between the two resolutions.

Contrary to the trend suggested by the behaviour of the 8-cube, the 16-cube has at least 2 very different solutions. For $T_0 = 0$ we obtain the weakly stratified solution with high diffusivity ratio $\gamma = r$ almost everywhere below the top interface and $\gamma = 1$ throughout most of the top interface. For $T_0 = 25$ we obtain a quite different steady solution with low diffusivity ($\gamma = 1$) in most of the southern part of the uppermost interface at $k = 15$, and a similar pattern at $k = 13$, with a smaller region of high density gradient $\gamma = 1$ confined to the western side of the domain and covering about one quarter of the horizontal layers at $k = 12$ and $k = 14$. Despite the different thermocline structure the meridional overturning streamfunctions for the two solutions are similar in form, with the maximum overturning reduced from 0.06 (80 Sv) for $T_0 = 0$ to 0.04 (55 Sv) for $T_0 = 25$.

Thus the phenomenon of multiple solutions resulting from variable vertical diffusivity is not restricted to the box model, or to low-order, box-like models but has a counterpart in relatively well-resolved FG model simulations. However at higher resolution the vertical structure appears to become less smooth. We discuss this fact, and the dependence on the form of the function $\kappa_v(G)$, in Section 9

7 Pole-to-pole circulation modes

The above results have demonstrated that under certain conditions the introduction of a variable vertical diffusivity can lead to the existence of multiple stable, steady states in a system which would otherwise have only a single steady solution. We now wish to consider the effect of variable vertical diffusivity in the FG model with competing thermal and saline forcings in a domain which spans the equator. It is well known that such a system has the potential to exhibit multiple solutions even when the diffusivity is

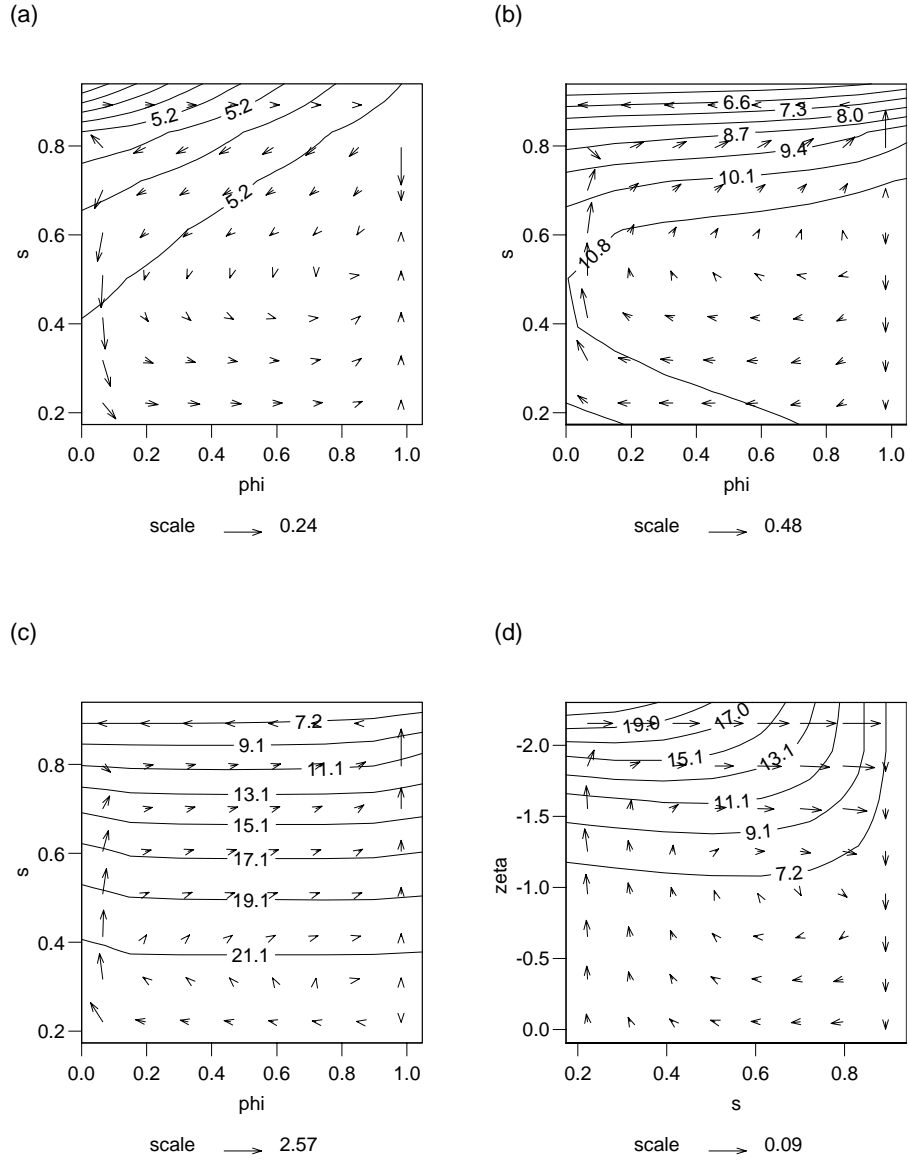


Figure 8: Contours of temperature and velocity arrows for a steady solution of the 8-cube with standard parameter values at model levels $k = 1$, abyssal (a); $k = 6$, (b) $k = 8$, surface (c) and mid-basin north-south section, (d). The logarithmic vertical coordinate $\zeta = \log(1 - z + 0.1)$, ϕ is longitude and s is $\sin(\text{latitude})$.

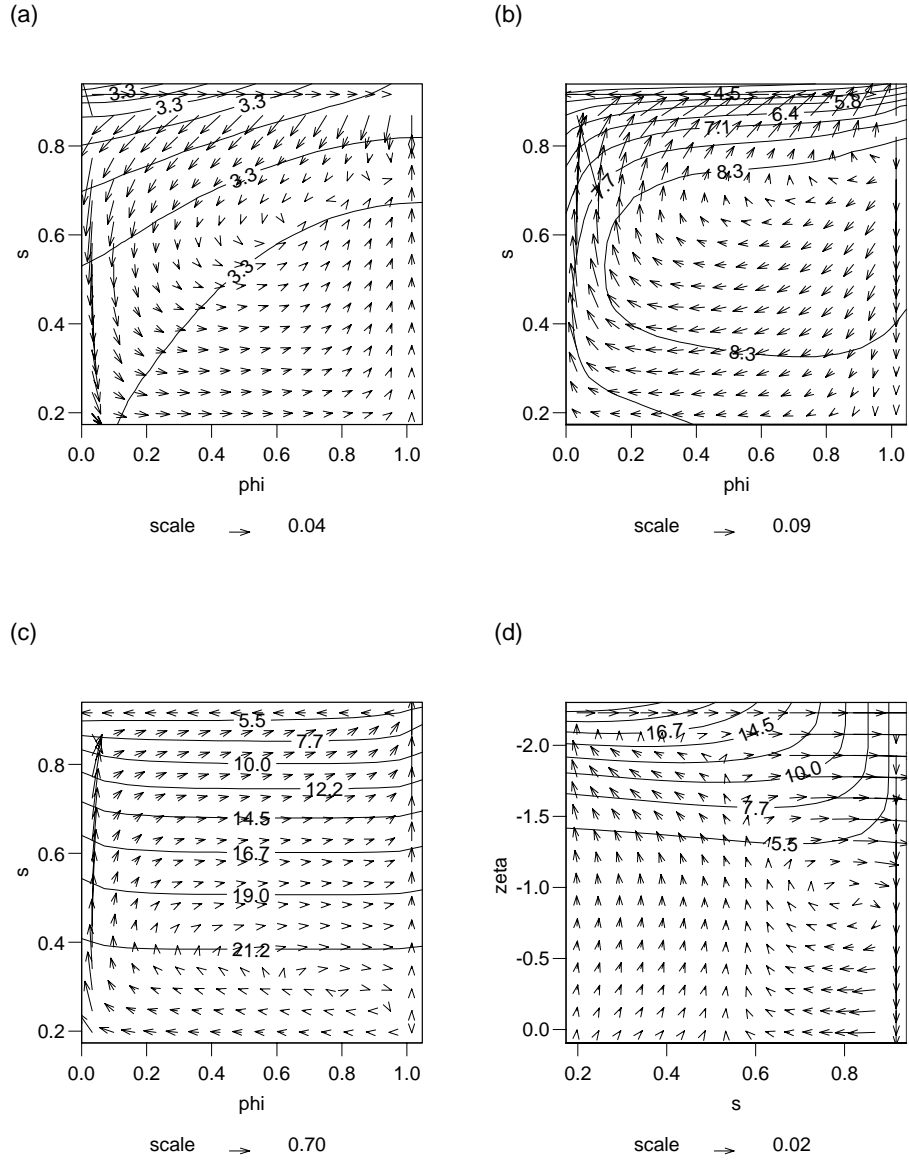


Figure 9: Contours of temperature and velocity arrows for a steady solution of the 16-cube with standard parameter values at model levels $k = 1$, abyssal (a); $k = 12$, (b) $k = 16$, surface (c) and mid-basin north-south section, (d). The logarithmic vertical coordinate $\zeta = \log(1 - z + 0.1)$, ϕ is longitude and s is $\sin(\text{latitude})$.

constant. With freshening at the poles, the saline forcing opposes the thermal forcing and introduces the possibility of a reversed circulation with sinking at the equator. Since this is true in either hemisphere there are four possible solutions, two symmetric about the equator and two asymmetric. The asymmetric solutions with the circulation reversed in only one hemisphere feature a single, pole-to-pole meridional circulation cell reminiscent of the present-day circulation in the Atlantic and Pacific. We are interested in the question of whether the possibility of reduced vertical mixing in stratified tropical waters favours pole-to-pole, asymmetric circulation modes.

The numerical parameters of the experiments are mostly as given in section 3 above, but to reduce problems related to the singularity of geostrophic flow at the equator the value of drag λ for the cross-equatorial simulations is twice that for the single-hemisphere runs. To allow us to perform a large number of very long integrations while still smoothly resolving the dominant circulation patterns, we are constrained to keep to a modest resolution of $16 \times 32 \times 8$ grid points in the eastward, northward and vertical directions respectively. To explore the variety of solutions possible under different conditions we will vary the strength of the saline forcing by changing the coefficient D in equation (14). The ratio D/D_0 of the salinity forcing coefficient to the value given in Table 1 will be denoted by R . We will also vary the initial conditions for the time integrations. We will keep to the simple function $\kappa_v(G)$ of equation (15) with $\kappa_{\min}=\kappa_{v0}$, $a = 10$ and $G_0 = 1$ but reduce the ratio r between the maximum and minimum values of κ_v from 100 to a less extreme value of 10. These parameters still allow this system to reach slightly different steady states even with no salinity forcing, but our aim in this section is to focus more on the effect of variable κ_v on multiple solutions whose existence is essentially due to the competition between thermal and saline forcing.

With constant diffusivity $\kappa_v \equiv \kappa_{v0}$ and relatively small salinity forcing we obtain a thermally dominated steady state with sinking at the poles. An example of the meridional streamfunction for such a solution is shown in Figure 10(a). This solution was obtained with a relative salinity forcing $R = D/D_0$ equal to 0.1 and an initial condition of constant temperature $T_0 = 25$ and constant salinity equal to 35. The solution is plotted at $t = 500$ (about 2000 years). For a larger value of R , equal to 0.6 for instance, and the same initial condition, the solution remains in a quasi-steady symmetric state until $t \approx 1200$ when it undergoes a rapid transition to an asymmetric state. The meridional streamfunction for this asymmetric solution at $t = 2500$ is shown in Figure 10(b). Since there is no explicit asymmetry in the system, the collapse of the symmetric circulation must be due to numerical noise at the machine error level, and indicates that the symmetric solution is unstable to extremely small asymmetric perturbations. In order to deliberately search for asymmetric solutions we have also performed experiments in which the initial condition is asymmetric. A clear asymmetric bias is obtained by setting the initial temperature to 25 south of the equator and 24 north of the equator. With this initial condition at $R = 0.6$ the solution becomes asymmetric much earlier, at $t \approx 250$. However with sufficiently small saline forcing the solution ultimately approaches a symmetric state even with such an initial condition. Similar behaviour is obtained for the same, asymmetric initial condition with variable κ_v ; symmetric solutions are obtained for weak salinity forcing while asymmetric solutions are obtained for stronger salinity forcing.

This is exactly the behaviour found by Thual and McWilliams (1992) using box models and two-dimensional models of the thermohaline circulation. They varied the thermal and saline forcing and compared the catastrophe structure (effectively the topology of appropriate bifurcation diagrams) for models of varying complexity. Since our models are three-dimensional, we cannot afford to map the corresponding catastrophe structure in

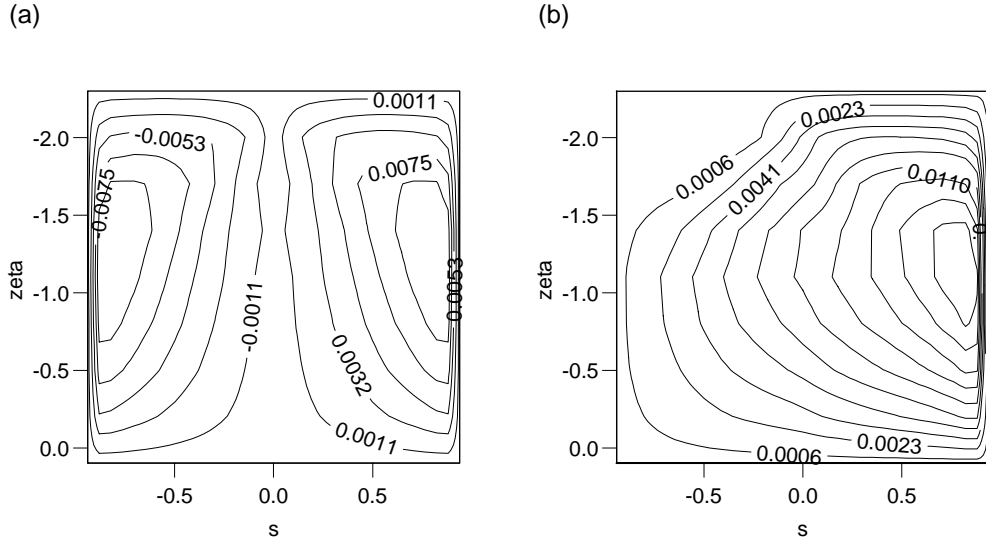


Figure 10: Meridional overturning streamfunctions for 2-hemisphere runs with constant κ_v . (a) $R = 0.1$, solution at $t = 500$. (b) $R = 0.6$, solution at $t = 2500$. The logarithmic vertical coordinate $\zeta = \log(1 - z + 0.1)$ and s is $\sin(\text{latitude})$.

the same detail as Thual and McWilliams, but we assume that the basic behaviour is the same; for low values of $R < R_1$, say, the solution will approach a symmetric, 2-cell, steady state. For larger values of $R > R_2$, say, solutions will approach an asymmetric, single-cell steady state, while for intermediate values $R_1 < R < R_2$ both solutions will exist. For even larger values of R the solution settles into a periodic flush-collapse cycle. We discuss this latter regime below. In this section we are interested in the effect of variable $\kappa_v(G)$ on the bifurcation points R_1 and R_2 , which reflect the degree to which the system favours the pole-to-pole mode. To address the question we first need to attempt to remove the effect of the absolute value of κ_v , since the persistence of the symmetric states is strongly affected by the value of κ_v , with increased κ_v leading to an increase in R_1 and R_2 . It therefore seems more informative to compare the behaviour of the variable $\kappa_v(G)$ model with solutions in which κ_v has a broadly similar variation with depth, but is fixed in time.

Examination of asymmetric, variable κ_v solutions for $R > 0.7$ shows that $\kappa_v(G)$ is closely approximated by the function $\kappa_v(z)$ given by

$$\kappa_v = \begin{cases} r \kappa_{\min}; & k \leq 4 \\ \kappa_{\min}; & k \geq 5 \end{cases} \quad (19)$$

where k is the vertical index of the stretched model grid. $k \leq 4$ corresponds roughly to the bottom half of the computational domain, which has 7 horizontal interfaces, and to the lowest 3/4 of the domain in physical space. It is therefore interesting to compare the results obtained when κ_v is given by (15) with those obtained using (19). For $R = 0.9$ the two formulations for κ_v give very similar steady states, the maximum values of Ψ_M in the two cases agreeing to within 1%.

We can minimise the effect of the initial condition by performing a series of runs in which we vary the bifurcation parameter R in small increments between the runs and initialise each run with the final state of the previous run. By increasing and then decreasing R in this way we are able to follow both symmetric and asymmetric solutions for as long as possible. The initial condition for the first run was the asymmetric state

with $T = 25$ for $s < 0$ and $T = 24$ for $s > 0$. Each individual run was continued to $t = 250$ (about 1000 years). We have followed this procedure for the FG model both with $\kappa_v(z)$ and $\kappa_v(G)$. The results are shown in Figures 7(a) and (b) respectively in which we plot the modulus of the maximum and minimum values of the meridional overturning streamfunction Ψ_M as a function of R . Figure 7(a) for the $\kappa_v(z)$ case shows a wide region where both symmetric and asymmetric solutions exist. From the graph we can estimate the values of the bifurcation points R_1 and R_2 as about 0.3 and 0.6 respectively. The Figure also shows that the sum of the absolute maxima of the streamfunctions in the two hemispheres varies smoothly through the transition point. Comparison with Figure 7(b) for the $\kappa_v(G)$ case suggests that, contrary to our original hypothesis, allowing κ_v to vary with time leads to an increase of R_1 and R_2 , which we can estimate from the graph as approximately 0.4 and 0.7 respectively. Thus the dependence of diffusion on stratification appears to favour the symmetric mode over the asymmetric mode. Interestingly, the system does not return to its initial state as R is reduced. The final symmetric state is essentially the same solution as that obtained with $\kappa_v(z)$, Ψ_M differing by less than 1% between the final states of the two experiments. The origin of the difference between the initial and final symmetric states in this experiment is the depth of the tropical thermocline region. In the initial symmetric steady state the strongly stratified region is shallower in the tropics than in mid-latitudes but there is another symmetric, steady state in which the structure of κ_v is essentially a function only of z , as in the asymmetric, pole-to-pole regime. The pronounced shoulders on the curve close to the bifurcation point R_1 are related to the finite length of integration; close to the bifurcation point the solutions have not always reached a steady state by time 250. We estimate a timescale for the unsteadiness of the solutions by calculating the root mean square rate of change of the dynamical variables. Away from the bifurcation points at the end of the runs this timescale is typically of order 10^6 .

8 Variable diffusivity in flush-collapse cycles

If the salinity forcing is increased further, the thermally-driven branch of the pole-to-pole circulation can be destabilised leading to the “polar halocline catastrophe” first noted by Bryan (1986). In our FG model this results in a periodic flush-collapse cycle in which a thermally-driven flushing phase, with strong high-latitude convection, is followed by a much longer phase, with only a shallow “collapsed” circulation and relatively uniform deep water, as discussed by Edwards *et al.* (1998).

This oscillatory regime provides the most striking example of the possible effect of variable vertical diffusivity. Using the same parameters as above ($\kappa_{\min}=\kappa_{v0}$, $a = 10$, $G_0 = 1$, $r = 10$) we have compared a simulation in which κ_v is a function of G , given by (15), with another in which κ_v is a function only of z , given by (19). For strong salinity forcing with $R = 1.2$ the time-dependent behaviour of the two runs turns out to be very different. It turns out that for this value of R , although the diffusivity in the $\kappa_v(G)$ run is still well approximated by a function only of z for most of the run, the agreement is better with the switch between small and large diffusivity slightly deeper than used above, hence the results shown in Figure 12 are for a run with κ_v given by

$$\kappa_v = \begin{cases} r \kappa_{\min}; & k \leq 3 \\ \kappa_{\min}; & k \geq 4 \end{cases} . \quad (20)$$

Figure 12 shows the value of the deep temperature averaged over the lower half of the computational domain (roughly the lower 3/4 in physical space), as a function of

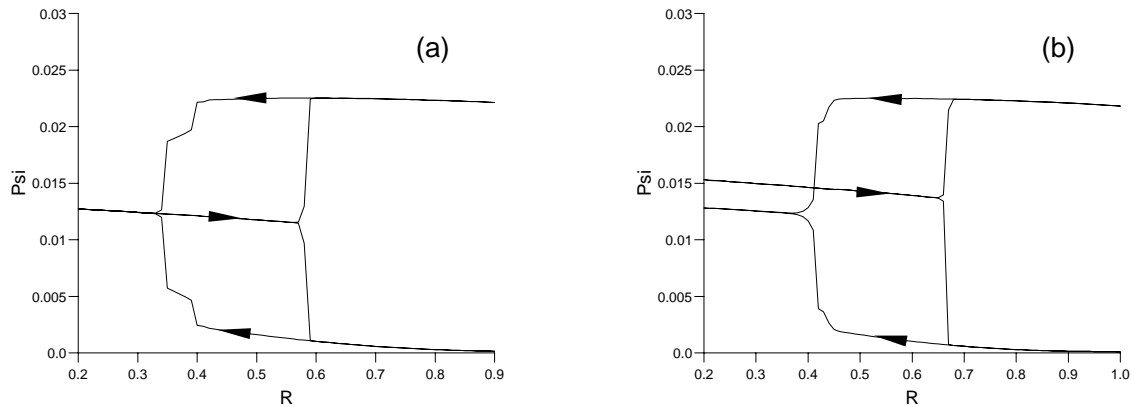


Figure 11: Bifurcation diagrams showing the moduli of the maximum and minimum values of overturning streamfunction Ψ_M for a series of 2-hemisphere runs with varying salinity forcing amplitude R . (a) κ_v a function only of z , (b) κ_v a function of density gradient G .

time, for the two simulations with salinity forcing R equal to 1.2. Both show evidence of the classic flush-collapse cycle. Deep temperature decreases rapidly during the flush, in which strong, 2-cell, thermally-driven advection and convection fills the lower half of the domain with cold water formed by surface forcing at high northern and southern latitudes. Strong salinity forcing steadily reduces the equator-to-pole density contrast which drives the flow, and the thermal flush ends when high-latitude freshening causes convection there to cease, signalling a switch to the collapsed phase. During the collapsed phase the deep temperature increases by vertical diffusion and also by relatively weak salinity-driven advection and convection in the tropics. The collapsed phase finally ends when the deep water has warmed sufficiently to overcome the stratification at high latitudes and massive convection initiates the return of the thermal flush. The two simulations behave similarly until the end of the collapsed phase but the flush occurs much earlier in the $\kappa_v(G)$ run, in which the oscillation period is around 500 (2000 years), compared with a period of around 750 (3000 years) in the $\kappa_v(z)$ run. The period of the oscillation is essentially determined by the timescale H^2/κ_v (see Edwards *et al.* 1998) for the vertical diffusion of heat from the surface to the deep. In the run with $\kappa_v(G)$ the process of reestablishing deep convection is greatly assisted by an increase of κ_v in the upper layers. Deep convection begins again when the region of increased κ_v penetrates from the surface layer to the unstratified water in the deep. The increase of κ_v which occurs is quite localised; within a time interval of about 25 (about 100 years) of the flush the relative diffusivity γ is still less than 1.2 at more than 85% of points in the top layer.

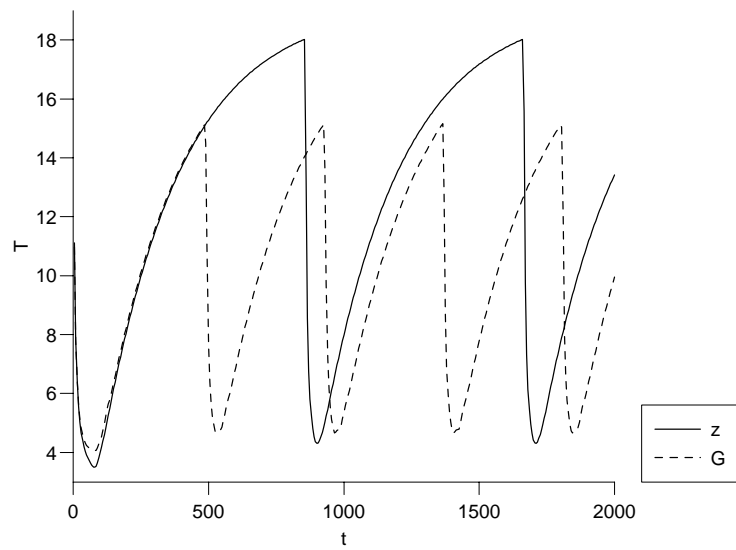


Figure 12: Deep temperature as a function of time with relative salinity forcing $R = 1.2$ for a run with $\kappa_v(G)$, dashed line; and a run with $\kappa_v(z)$, solid line.

9 Discussion

The correct form for the function $\kappa_v(G)$ is not well known, indeed recent measurements by Polzin *et al.* (1997) show that vertical diffusivity in the ocean varies by several orders of magnitude, but the reasons for this variation are still unclear. In the real ocean the diapycnal diffusivity is likely to depend on other factors besides the static stability, including the nature of the bottom topography, the mean shear and the flow history, and the potential for double-diffusive mixing. It is clearly a considerable oversimplification to assume that the diapycnal diffusivity can be written as a function only of the vertical density gradient. By using an existing frictional geostrophic model in order to focus on very long time and space scales we are further constrained to study the effect of variable vertical diffusivity rather than the more physically sensible diapycnal diffusivity. Given the uncertainty about the most realistic form for $\kappa_v(G)$, it is appropriate to restrict our consideration merely to a simple form which appears plausible. In practice this means that we use the tanh function defined in equation (15), which decreases as the density gradient increases, and consider ratios r of 100 or less between maximum and minimum values of κ_v . We thus have four variable parameters: the minimum value κ_{\min} , the ratio r and two parameters a and G_0 which determine the slope and position of the changeover between large and small diffusivities. We have considered a range of cases to investigate how the existence of multiple solutions in the model depends on the parameters r , a and G_0 . The value of κ_{\min} is constrained to some extent by numerical stability and is set to the standard value used earlier, except where stated.

For each set of parameters we have compared steady solutions obtained starting from the two extreme initial conditions $T_0 = 0$ and $T_0 = 25$ in both the 2-cube and the 16-cube. The results are summarised in Table 2. For the 16-cube, the smoother variation of solutions demands that we define when solutions are distinct. For the purposes of Table 2 we have arbitrarily defined the cold-start and hot-start solutions to be different if the maximum values of Ψ_M in the two cases differ by more than 5%. The ratio of the maximum value of Ψ_M in the cold-start solution to that in the hot-start solution is also given in the Table. Note that the small differences between the final solutions to the 16-cube in experiments 6, 7 and 9 do not appear to be due to residual unsteadiness. At the end of the runs the estimated timescale for unsteadiness is typically greater than 10^6 and increasing.

For the 2-cube, the cases in which we have found multiple solutions are exactly those in which the graph of the function $\kappa_v(G)$ has multiple intersections with the graph of $G(\kappa_v)$ derived in section 5, as expected. Experiments 2 and 4 show that for large r the 16-cube exhibits multiple solutions for a broader range of values of slope parameter a and crossover point G_0 . For the remaining experiments in the Table the choice of G_0 has been guided by comparison of the graphs of $\kappa_v(G)$ and $G(\kappa_v)$ in an attempt to find multiple solutions where possible.

Experiments 6 and 9 show that the large ratio r between maximum and minimum diffusivities is not a prerequisite for multiple solutions in the 2-cube. In the 16-cube it is more difficult to find multiple solutions for $r < 100$, but the results of experiment 7 and of the hysteresis experiment of section 7 show that multiple solutions can still be obtained for $r = 10$ in well-resolved simulations in some circumstances. It is also possible to obtain multiple solutions with a more gradual change between large and small diffusivities, that is for smaller values of a than those used in the previous sections. In the 16-cube we were able to obtain multiple solutions for an even smaller slope parameter a than in the 2-cube. Solutions with $a \approx 1$ or less also have much smoother interior variations in κ_v than those

Table 2: The dependence of the existence of multiple solutions on the parameters of the function $\kappa_v(G)$. The (scaled) value of κ_{\min} was set to κ_{v0} except in experiments 9 and 10 where it was increased by a factor of 20. See text for explanation.

exp't	r	a	G_0	2 solutions in 2-cube?	2 solutions in 16-cube?	overturning ratio	F'/κ_{\min}
1	100	10	1.5	yes	yes	1.44	700
2	100	1	1.5	no	yes	1.44	50
3	100	1	1	yes	yes	1.51	33
4	100	0.5	0.5	no	yes	1.36	13
5	100	0.1	0.5	no	no	1.00	9.7
6	10	10	3	yes	no	1.02	130
7	10	1	3	no	yes	0.84	9.4
8	10	0.5	3	no	no	1.00	3.7
9	2	10	1.2	yes	no	0.97	4.5
10	2	1	1.2	no	no	1.00	-0.6

discussed earlier, with relative diffusivity values γ significantly different from 1 and r at most points.

Clearly the number and spatial complexity of possible steady solutions increases with n , but certain solutions are more likely than others, in the sense of attracting a wider range of initial conditions. For instance there are more than 4 steady solutions to the 4-cube, since by careful searching we find that the initial temperature $T_0 = 13.79$ generates, in the notation used earlier, the steady solution

$$\begin{pmatrix} r & r & r & r \\ r & r & r & r \\ r & r & 1 & 1 \\ 1 & 1 & 1 & 1 \end{pmatrix}. \quad (21)$$

Solutions to the 16-cube can have much more structure than, say, the 2-cube solutions. Some solutions, for instance, have two distinct, high-gradient layers at different depths. The persistence of vertical structure with increased vertical resolution raises the issue of convergence. A pair of appropriately matched experiments with 16 and 32 vertical levels did show a similar 2-layer structure, but in general we cannot expect simulations to converge with increasing resolution without a thorough understanding of the scaling behaviour of the sub-grid scale processes being modelled by the diffusive parameterizations. In the case of variable vertical diffusivity there is a deeper mathematical problem involved; the existence of multiple states when vertical mixing depends on vertical density gradient is analogous to the phenomenon of layering in stratified fluids discussed by Balmforth *et al.* (1998). The layering instability can be understood in terms of the relationship between the vertical density flux $F = -\kappa_v G$, and the density gradient G . If the flux increases with density gradient, $F'(G) > 0$, in a region of uniform G , then a small perturbation which increases the density gradient will lead to an increase of flux, thus further increasing the gradient. This instability can allow the system to bifurcate between solutions and the existence of regions where $F'(G) > 0$ may therefore provide a necessary condition on the function $\kappa_v(G)$ for the existence of multiple solutions. The maximum value of $F'(G)/\kappa_{\min}$, obtained numerically, is given in Table 2 for the functions

tested and is indeed negative only in experiment 10 in which multiple solutions were not found.

If the flux F increases indefinitely with G then there is no mechanism to arrest the steepening of the resulting layers. In our system the diffusivity drops from one constant value to another as G increases, thus there can only be a finite range of G where $F' > 0$. Consequently, in our system, there is a maximum steepness for the layers. However the growth rate of the initial instability increases with vertical wavenumber, hence if F' becomes positive in a finite region, layering is likely to occur at grid scale in a numerical simulation. Further changes in G may, however, lead to the amalgamation of these layers, as has occurred locally in the 16-cube simulation described above. In the low-dimensional n -cube simulations the stratified layers can be taken to represent single, or potentially split, thermocline regions. To simulate the small-scale layering at very high resolution it would be necessary to use a higher order turbulence closure. Balmforth *et al.* use a “ k - l ”, single equation, closure which allows them to resolve the layering using 4000 vertical modes. It should be noted, however, that in three dimensions other effects may damp or obscure the layering. Interestingly, the scheme used by Balmforth *et al.* is very similar to that used by default in the OPA OGCM with only 31 vertical levels, see for example Blanke and Delecluse (1993).

Another point worthy of note is that our numerical experiments in effect involve a systematic generalisation of the common procedure of setting vertical diffusion to a very large value wherever the stratification is unstable or neutral, and to a very low value elsewhere. Our results are therefore linked to the existence of multiple thermohaline states with different convection patterns found by, for example, Lenderink and Haarsma (1994).

The possibility that the mechanism seen in the box model of Section 2 could correspond to similarly dramatic changes of regime in the real ocean, seems, in our hesitant opinion, not very likely during recent geological times (Pliocene / Pleistocene). It could perhaps have been a factor if and when the ocean circulation was wholly different (e.g. during the Cretaceous, perhaps) but this is pure speculation. On the other hand, in the time-dependent, flush-collapse states investigated in Section 8, a dramatic difference in the time-dependent behaviour which occurs under strong saline forcing can be obtained depending on how relatively small variations in diffusivity are parameterized. For instance, we found an order 1 difference between the oscillation period in a run with diffusivity varying only very weakly with stability G (using the parameters $r = 2$, $a = G_0 = 0.5$, $\kappa_{\min} = 2 \times \kappa_{v0}$, $R = 2$) and an appropriate comparison run with only spatial variation of diffusivity. The oscillation periods were around 600 and 900 respectively. For these parameters the maximum value of the flux gradient F' is -0.8, thus the diffusivity varies less rapidly than $1/G$. As discussed in the introduction it is not yet clear whether spatial or stability-dependent variation is more realistic but our results show that the distinction could be very significant for climate models. In particular these results suggest that oscillations between different thermohaline states and by extension the existence and stability of multiple equilibria such as those found by numerous authors including Winton and Sarachik (1993) and Sakai and Peltier (1997), could also depend on the assumptions made concerning the variation with stratification of vertical diffusivity in the models.

10 Conclusions

Motivated by recent observations (Polzin *et al.* 1997, Watson *et al.* 1999) which have shown that diapycnal mixing rates can vary by several orders of magnitude, we have investigated the effects of variable mixing rate in a hierarchy of simple models of the thermohaline circulation in a closed, rectangular basin. Since the relationship between diapycnal mixing rates and large scale ocean fields is, as yet, poorly known, we have parameterized the relationship as a simple dependence of the vertical diffusivity on the strength of the local vertical stratification.

In a simple box model with a single active tracer, such a dependence is found to permit the existence of two stable equilibrium states; one solution has weak stratification, large diffusivity and strong overturning while the other has strong stratification, small diffusivity and weak overturning. Related behaviour is shown to exist in well-resolved frictional geostrophic simulations. However, the gap in complexity between such simulations and our box model, with only one degree of freedom, makes the connection less than obvious. To bridge this gap we have created a hierarchy of FG models by varying the resolution while making appropriate modifications to the dynamics. The simplest member of the hierarchy, an 8-cell cube, is shown to produce reasonable thermohaline solutions and to mimic the behaviour of the box model in producing two steady solutions. However it has just sufficient complexity to allow the meridional overturning to be determined via geostrophic dynamics and the relative magnitudes of the overturning rates in the two solutions are consequently reversed. Using a particular form for the dependence $\kappa_v(G)$, the multiplicity of solutions initially increases with increasing complexity in the model hierarchy, then subsequently decreases, with differences between solutions becoming restricted to a thin layer at the surface. Multiple solutions reappear in better-resolved simulations and the multiple states of the box model are seen to correspond to a layering instability, unresolved in commonly used ocean models, a detailed analysis of which would require higher order closure and higher resolution than is currently possible. Sensitivity experiments and physical arguments indicate that the existence of multiple states due to variable diffusivity requires that the diffusivity be a strong function of stability, varying more rapidly than $1/G$ (in the sense that the flux $F = -\kappa_v G$, increases with G) for some range of G and changing by a factor of at least 10 or 100 between maximum and minimum values of κ_v . This is related to the fact that, in our model, when κ_v is held fixed, the variation of G with κ_v is relatively weak.

We have also studied the bifurcation between equatorially symmetric and antisymmetric, pole-to-pole circulation modes in a two-hemisphere version of the FG model with variable saline forcing included. The results show that, contrary to our original hypothesis, allowing the diffusivity to vary with stability marginally favours the symmetric mode over the asymmetric mode. Finally, we have demonstrated the profound effect that variable diffusivity can have on the period of oscillations in the flush-collapse cycle which pertains under strong saline forcing. In particular the period of oscillations in runs with spatially varying diffusivity can be very different from that in runs with diffusivity varying, even weakly, with stability.

Appendix. Numerical constraints on the frictional geostrophic model

The FG model with $\mu = 0$ and constant diffusivity cannot straightforwardly satisfy all the required boundary conditions. The no-flow condition implies a relation between the normal ρ_n and tangential ρ_l derivatives of density ρ at the boundary

$$\lambda\rho_n + s\rho_l = 0. \quad (22)$$

Recall that λ is the frictional drag and $s = \sin(\text{latitude})$ is the dimensionless Coriolis parameter. This makes it impractical to impose a condition on ρ_n , to ensure zero diffusive flux across the boundary, because the tangential derivative ρ_l is effectively determined by the interior solution. Edwards (1996) describes how, by postulating a spatially variable diffusivity, it is possible to impose a condition of zero normal heat and salt fluxes and still obtain a well-posed problem. Here we use the alternative approach suggested by Samelson and Vallis (1997) who describe how the introduction of a biharmonic diffusion term $\mu\nabla^4$ makes it possible to maintain zero normal diffusive flux by arranging for the harmonic and biharmonic contributions to cancel. Equation (22) can then be used to define the normal derivative at the boundary and hence the adjacent land-point density values required to obtain the tangential velocity value adjacent to the boundary. The result is an integral constraint on a set of dummy values of density at land points across the ocean boundary which are therefore found by the solution of a set of simultaneous linear equations. At each corner of the domain an additional land-point value of density must be defined. This can be done in a variety of ways which have the same stability characteristics but lead to slightly different interior solutions. Samelson and Vallis (pers. comm.) apply a version of equation (22) with the normal direction at the corner defined to be the diagonal of the corner grid cell. We use a similar procedure, since it was found to lead to smoother interior solutions than other forms we have tested, but note that the normal direction is harder to define with variable resolution in the two horizontal directions.

The choice of boundary condition has profound implications for the stability of the numerical scheme, since the governing thermocline equations are susceptible to a severe timestep restriction arising from the purely numerical boundary wave found by Killworth (1987). This wave can result if the normal velocity is set to zero without forcing the (dynamical) density field to explicitly satisfy (22). When the integral boundary condition arising from (22) is used the interior flow can respond directly to the presence of the boundary and the wave, along with the resulting timestep restriction, is removed. Note that this remains true even when the equation of state is nonlinear, in which case the condition on density, equation (22), is applied instead to temperature and salinity separately, and the relation (22) for density does not exactly hold. As noted earlier we use a simpler boundary condition at low resolution when the numerical wave does not cause problems (the wave speed is inversely proportional to the grid spacing). Note also that in practice we set the diffusive flux at the boundary to zero but ignore the biharmonic diffusion term, since any value of μ is sufficient in theory to allow the flux to be set to zero but in practice small values (required for stability) do not make an observable difference to the solution. With a grid spacing of about 3 degrees the use of the integral boundary condition results in a roughly 6-fold increase of the maximum possible dimensional timestep in single hemisphere runs to around one week.

An even greater improvement, around 20-fold, is obtained in cross-equatorial runs at similar resolution by altering the time-stepping procedure. The modification involves

relaxing the velocity (which is a prognostic variable) back to the value at the previous timestep. Thus if \mathbf{u}_p is the velocity derived from the density structure in the usual way at time t , the velocity used by the code is $\mathbf{u}(t) = (1 - \delta)\mathbf{u}_p + \delta\mathbf{u}(t - \Delta t)$, where the optimum value of the relaxation parameter δ is about 0.9. Effectively we have reintroduced a form of Kelvin wave into the dynamics. This apparently results in a much more stable code close to the equator than the original system in which the Kelvin wave speed is formally infinite.

REFERENCES

- Balmforth, N. J., Llewellyn-Smith, S. G. and Young, W. R. 1998. Dynamics of interfaces and layers in a stratified turbulent fluid. *J. Fluid Mech.*, **355**, 329–358.
- Blanke, B. and Delecluse, P. 1993. Variability of the tropical Atlantic Ocean simulated by a general circulation model with two different mixed layer physics. *J. Phys. Oceanogr.*, **23**, 1363–1388.
- Bryan, F., 1986. High-latitude salinity effects and interhemispheric thermohaline circulations. *Nature*, **323**, 301–304.
- Bryan, F., 1987. Parameter sensitivity of primitive equation ocean general circulation models. *J. Phys. Oceanogr.*, **17**, 970–985.
- Edwards, N. R., 1996. Unsteady similarity solutions and oscillating ocean gyres. *J. Mar. Res.*, **54**, 793–826.
- Edwards, N.R., Willmott, A.J. and Killworth, P.D. 1998. On the role of topography and wind stress on the stability of the thermohaline circulation. *J. Phys. Oceanogr.*, **28**, 756–778.
- Garrett, C. J. R. and Munk, W. H. 1975. Space-time scales of internal waves: a progress report. *J. Geophys. Res.*, **80**, 291–297.
- Gill, A. E., 1982. *Atmosphere-ocean dynamics*. Academic Press, 662 pp.
- Huang, R. X. 1999. Mixing and energetics of the oceanic thermohaline circulation. *J. Phys. Oceanogr.*, **29**, 727–746.
- Huang, R. X. and Stommel, H. M. 1992. Convective flow patterns in an eight-box cube driven by combined wind stress, thermal and saline forcing. *J. Geophys. Res.*, **97**, 2347–2364.
- Killworth, P. D. 1987. A continuously stratified nonlinear ventilated thermocline. *J. Phys. Oceanogr.*, **17**, 1925–1943.
- Ledwell, J. R., Watson, A. J. and Law, C. S. 1993. Evidence for slow mixing across the pycnocline from an open-ocean tracer-release experiment. *Nature*, **364**, 701–703.
- Ledwell, J. R., Watson, A. J. and Law, C. S. 1998. Mixing of a tracer in the pycnocline. *J. Geophys. Res.*, **103**, 21499–21529.
- Lenderink, G. and R. J. Haarsma, 1994. Variability and multiple equilibria of the thermohaline circulation, associated with deep water formation. *J. Phys. Oceanogr.*, **24**, 1480–1493.

- Manabe, S. and Stouffer, R. J. 1999. Are two modes of thermohaline circulation stable? *Tellus*, **51A** 400-411.
- Munk, W. H. 1966. Abyssal recipes. *Deep Sea Research*. **13**, 707–730.
- Munk, W and Wunsch, C. 1998. Abyssal recipes II: energetics of tidal and wind mixing. *Deep Sea Res.*, **45**, 1977–2010.
- Polzin, K. L., Toole, J. M., Ledwell, J. R. and Schmitt, R. W. 1997. Spatial variability of turbulent mixing in the abyssal ocean. *Science*, **276**, 93–96.
- Sakai, K. and Peltier, W.R. 1997. Dansgaard-Oeschger Oscillations in a Coupled Atmosphere-Ocean Climate Model. *J. Climate*, **10**, 949-970.
- Samelson, R. M. and Vallis, G. K. 1997. A simple friction and diffusion scheme for planetary geostrophic basin models. *J. Phys. Oceanogr.*, **27**, 186–194.
- Stommel, H. M. 1961. Thermohaline convection with two stable regimes of flow. *Tellus*, **13**, 224–230.
- Thual, O. and McWilliams, J. C. 1992. The catastrophe structure of thermohaline convection in a two-dimensional fluid model and a comparison with low-order box models. *Geophys. Astrophys. Fluid Dynamics*, **64**, 67–95.
- Watson, A. J. *et al.* (17 authors) 1999. Mixing and convection in the Greenland Sea from a tracer-release experiment. *Nature*, **401**, 902–904.
- Winton, M. and Sarachik, E. 1993. Thermohaline oscillations induced by strong steady salinity forcing of ocean general circulation models. *J. Phys. Oceanogr.*, **23**, 1389–1410.